Structure and dynamics of nano-sized raft-like domains on the plasma membrane

Fernando E. Herrera and Sergio Pantano

Related Articles

Stable, biocompatible lipid vesicle generation by solvent extraction-based droplet microfluidics
Biomicrofluidics 5, 044113 (2011)

Configuration of membrane-bound proteins by x-ray reflectivity
J. Appl. Phys. 110, 102215 (2011)

Continuous distribution model for the investigation of complex molecular architectures near interfaces with scattering techniques
J. Appl. Phys. 110, 102216 (2011)

Electron-beam direct processing on living cell membrane
Appl. Phys. Lett. 99, 174102 (2011)

Atomic force microscopy of electrospun organic-inorganic lipid nanofibers
Appl. Phys. Lett. 99, 103702 (2011)

Additional information on J. Chem. Phys.

Journal Homepage: http://jcp.aip.org/

Journal Information: http://jcp.aip.org/about/about_the_journal

Top downloads: http://jcp.aip.org/features/most_downloaded

Information for Authors: http://jcp.aip.org/authors

Structure and dynamics of nano-sized raft-like domains on the plasma membrane

Fernando E. Herrera[1,2] and Sergio Pantano[1,a)]

[1]*Institut Pasteur de Montevideo, Calle Mataojo 2020, CP 11400 Montevideo, Uruguay*
[2]*Consejo Nacional de Investigaciones Científicas y Técnicas (CONICET), Departamento de Física, Facultad de Bioquímica y Ciencias Biológicas, Universidad Nacional del Litoral, C.C. 242, Ciudad Universitaria, C.P. S3000ZAA, Santa Fe, Argentina*

Cell membranes are constitutively composed of thousands of different lipidic species, whose specific organization leads to functional heterogeneities. In particular, sphingolipids, cholesterol and some proteins associate among them to form stable nanoscale domains involved in recognition, signaling, membrane trafficking, etc. Atomic-detail information in the nanometer/second scale is still elusive to experimental techniques. In this context, molecular simulations on membrane systems have provided useful insights contributing to bridge this gap. Here we present the results of a series of simulations of biomembranes representing non-raft and raft-like nano-sized domains in order to analyze the particular structural and dynamical properties of these domains. Our results indicate that the smallest (5 nm) raft domains are able to preserve their distinctive structural and dynamical features, such as an increased thickness, higher ordering, lower lateral diffusion, and specific lipid-ion interactions. The insertion of a transmembrane protein helix into non-raft, extended raft-like, and raft-like nanodomain environments result in markedly different protein orientations, highlighting the interplay between the lipid-lipid and lipid-protein interactions. © *2012 American Institute of Physics.* [doi:10.1063/1.3672704]

INTRODUCTION

The early ideas about composition, partition, and dynamics of the plasma membrane have undergone a continuous transformation during the last years. The view of a rather homogeneous two-dimensional media where their components may freely diffuse[1] has been replaced by the conception of a highly structured assembly with thousands of species[2] whose physicochemical characteristics drive their spatial segregation. In particular, cholesterol and sphingolipids are able to form domains that are usually resistant to the solubilization by detergents called lipid "rafts".[3] These domains have been proposed to function as platforms for the recruitment and localization of specific proteins,[4,5] although their real biological function and even their existence have raised some controversy.[6–8] This probably due to the fact that direct visualization of these small and highly dynamic domains in the complex environment of a cellular membrane is a very challenging task, the highest resolution picture of a binary lipid mixture so far was ∼50 nm using tip-enhanced Raman images.[9]

Lipid rafts tend to be thicker than the adjacent areas due to an ordering effect exerted by cholesterol on its neighboring lipid chains and to the more extended saturated hydrocarbon chains of the sphingolipids.[10] The raft regions can form patches in the plasma membrane with sizes varying from 5 nm to 200 nm,[11–14] with the smallest dimensions below the resolution of the best direct visualization method.[9]

The development of single-molecule tracking techniques has notably enriched our understanding of the diffusion, interactions, and signaling within the plasma membrane.[15–17] The increasing level of detail acquired by these techniques has added a new layer to the complexity of the plasma membrane leading to a model of compartmentalization driven by membrane-cytoskeleton interactions.[18] These data have led to a model in which the cytoskeleton creates a mesh with a variable size between ∼30 nm and ∼200 nm which limits the diffusion of lipids and proteins.[19] In particular, the actin-binding protein Filamin A has been shown to mediate interactions with the CD28 receptor concentrating and trapping rafts at the immunological synapses upon T-cell stimulation.[20] Unfortunately, due to the highly dynamic and complex character of these molecular systems, direct structural and dynamical information is still scarce. The lowest spatiotemporal resolution limits remain nowadays approximately at 10 nm and 25 μs.[15] However, computer simulations, and in particular molecular dynamics (MD) simulations, have proven to be a reliable alternative to furnish insights in the nanometer and ps–μs spatiotemporal ranges of a number of raft-like systems.[21–23]

In this work, we aim to study at atomistic detail the structure and dynamic characteristics of a nano-sized raft-like domain immersed in a non-raft membrane environment. We addressed two main questions: (i) Do such small domains keep their distinctive structural/dynamical properties? (ii) Are they able to modulate interactions with membrane proteins?

To address these questions we constructed a raft-like nanodomain of around 6 nm size immersed in a non-raft environment of around 12 nm. This setup minimally resembles a single compartment within the plasma membrane. We used MD

a)Author to whom correspondence should be addressed. Electronic mail: spantano@pasteur.edu.uy. Tel.: +598-2522 09 10. Fax: +598-2522 41 85.

simulations to furnish atomic detail at the sub-μs timescale. Aimed to keep the simulation conditions as close as possible to the reality, we have considered not only a multicomponent lipidic system but also different species and concentrations of electrolytes in the aqueous solution surrounding both sides of the membrane.

To establish a reference level, the simulations of a raft-like patch were compared against extended raft-like and non-raft membrane. The non-raft model membranes were composed by 1-palmitoyl-2-oleoyl-sn-glycero-3-phosphocholine (POPC), 1-palmitoyl-2-oleoyl-sn-glycero-3-phosphoethanolamine (POPE), and 1-palmitoyl-2-oleoyl-sn-glycero-3-phosphoserine (POPS). These three species minimally represent the three main components of the extracellular (POPC) and intracellular (POPE and POPS) plasma membrane of typical mammalian erythrocytes.[24,25] The raft-like regions were composed by cholesterol (CHOL) and N-palmitoyl-D-erythro-sphingosyl phosphorylcholine (SGML) and phosphocholine lipids in a nearly 1:1:1 proportion.[26]

The small number of species is clearly an over simplification of the physiological scenario. This is derived partially from the rather fuzzy information about the molecular content of biomembranes but also from the relatively reduced dimensions treatable by MD simulations. Finally, we analyzed membrane-protein interactions by performing simulations of an α-helix corresponding to the transmembrane segment of the CD28 receptor inserted in the non-raft, extended raft-like and raft-like nanodomain environments.

Besides the expected increment of the thickness and ordering observed for the raft-like region, our results also suggest a marked depletion in the membrane-electrolyte interaction for this region. This results in a reduction of the transmembrane potential into the raft-like region. Furthermore, we found that even the small raft-like nanodomains show similar structural characteristics as the ones observed for a bigger and more extended raft-like membrane. Additionally, the orientation within the bilayer of a CD28 transmembrane helix suffers marked changes in response to the adaptation to the hydrophobic mismatch of the protein and the lipidic environment,[27] suggesting that even nano-sized cholesterol rich domains (CRDs) can accommodate typical raft proteins almost as well as extended raft domains.

METHODS

Dealing with heterogeneous membrane systems is a non-trivial problem since: (i) free electrolytes (specially sodium and calcium) may adsorb onto the membrane reducing the area per lipid, increasing the thickness, and reducing the lateral diffusion;[28] (ii) ions may associate differentially with phospholipids and cholesterol according to their physical/chemical features;[29–31] (iii) mixing of different lipidic species may alter the membrane characteristics in a concentration dependent manner;[23,32,33] (iv) stacking of membrane's monolayers with different surfaces result in a membrane tension artifact, which cannot be relaxed (see discussion in Refs. 28,34, and 35). Therefore, aimed to dissect all the possible effects related to the heterogeneity of the systems, prelim-

inary simulations were conducted first on symmetric bilayers on each component of the system separately to then determine the correct number of molecules on each leaflet.[35] This correction is crucial when treating with asymmetric membrane systems. We used the information from these preliminary simulations to set the molecular content of our representation of the plasma membrane.

Simulated systems

System I: Non-raft plasma membrane (I, Ia, and Ib)

System Ia: Extracellular leaflet. This simulation was performed to determine the effect of a physiological electrolyte concentration on the extracellular leaflet of the plasma membrane and determine the effective area per lipid under the conditions of the simulation. Combination of the results of this simulation with those from *System Ib* (see below) will allow setting the number of lipids in both bilayers. The extracellular leaflet is represented by 64 POPCs, which is the main component of eukaryotic cells,[26] solvated by around 2500 water molecules on each leaflet. Both leaflets are in contact with a total number of 28 pairs of NaCl, 4 of Ca$_2$Cl, and 4 of KCl (Table I). Initial coordinates were taken from Ref. 29.

System Ib: Intracellular leaflet. This simulation was performed to determine the effective area per lipid of a mixture of POPE/POPS at near physiological electrolyte concentration on the cytosolic side of the plasma membrane. To represent this part of the membrane we constructed a symmetric bilayer composed by a mix of POPE and POPS (42 and 22, respectively, on each leaflet). The initial coordinates were taken from Ref. 36. Simulations on *System Ib* were performed on a symmetric system in presence of 40 K$^+$ and 4 Na$^+$ (Table I), which neutralize the charge of POPS. The relative concentration of each of the species roughly represents the intracellular concentration in a typical mammalian cell.[25]

System I: Non-raft bilayer. It was built by stacking two monolayers, one from *System Ia* and one from *System Ib*. The last 50 ns of each of the above systems (see simulation details) were used to calculate the effective area per lipid, which resulted in 60.3 $\pm$ 2.1 Å^2 and 52.9 $\pm$ 1.4 Å^2 for the extra- and intracellular leaflets, respectively. To match the areas of both bilayers we used 57 (POPCs) and 64 (44 POPEs and 22 POPSs) lipids at the extra- and intracellular monolayers, respectively (Table I). This model of the non-raft plasma membrane was simulated in the presence of asymmetric ionic concentrations (Table I).

System II: Extended raft-like plasma membrane (IIa, IIb, and IIc)

Following the same strategy used for the non-raft membrane, preliminary simulations were conducted to determine the effective size of the membrane patch owing to the mixing of components and the presence of physiological ionic concentration. The raft system was modeled as a symmetric membrane with each leaflet composed by 27 molecules

TABLE I. Composition of the different systems. The simulated times in the last column refer to the length of the production runs. The ions restricted using the BRIM scheme[28] are shown in bold.

Membrane side	DOPC	SGML	CHOL	POPC	POPE	POPS	SOL	Na$^+$	K$^+$	Ca^{2+}	Cl$^-$	ns of MD
System Ia												
Both	...	...	...	128	...	...	5226	28	4	4	40	100
System Ib												
Both	...	...	...	...	84	44	5436	4	40	...	...	100
System I												
Extra	...	...	...	57	...	...	5405	**14**	2	**2**	20	250
Intra	...	...	...	...	42	22		2	**20**	...	...	
System IIa												
Both	54	44	50	...	...	...	5586	...	...	...	...	100
System IIb												
Both	54	44	50	...	...	...	5563	28	4	4	40	100
System IIc												
Both	54	44	50	...	...	...	5571	4	28	...	32	100
System II												
Extra	27	22	25	...	...	...	5586	**14**	2	**2**	20	250
Intra	27	22	25	...	...	...		2	**14**	...	16	
System II$_S$												
Extra	27[a]	22	25	...	...	...	5586	**14**	2	**2**	20	250
Intra	27[a]	22	25	...	...	...		2	**14**	...	16	
System III												
Extra	27	22	25	171	...	...	21 485	**56**	8	**8**	96	400
Intra	27	22	25	...	126	66		8	**74**	...	...	
System III$_S$												
Extra	27[a]	22	25	171	...	...	21 485	**56**	8	**8**	96	100
Intra	27[a]	22	25	...	126	66		8	**74**	...	...	

[a] In these systems DOPC is replaced by DSPC.

of DOPC, 22 molecules of SGML, and 25 molecules CHOL. The initial configuration was taken from Ref. 26.

System IIa. To establish a reference level regarding the influence of different electrolytes with this raft-like membrane patch we performed a first simulation in absence of added salts.

Systems IIb and IIc. Subsequently, the same lipid bilayer was simulated in the presence of added salts roughly mimicking the extra- and intracellular conditions (Systems IIb and IIc, respectively). Concentrations and number of lipids in each leaflet are reported in Table I.

Extended raft-like bilayer (Systems II and II$_S$). Calculations on *Systems IIa, IIb,* and *IIc* showed almost no interactions of the added salts with the membrane's components and, in consequence, no significant structural/dynamical effects on the bilayer. Hence, we simulated our model of the raft-like plasma membrane at nearly physiological conditions (*System II*) by adding, like for *System I*, NaCl and Ca$_2$Cl to the extracellular leaflet and KCl to the intracellular one, but using the same number and lipid species at both sides.

To study the effect of saturated versus unsaturated species we generated a second model of a raft-like membrane patch. With this aim, we substituted the double bonds in DOPC for single bonds to yield the completely saturated 1,2-distearoyl-sn-glycero-3-phosphocholine (DSPC, *System II$_S$*).

System III: Nano-sized raft-like on the plasma membrane (III and III$_S$)

Raft-like nanodomain (Systems III and III$_S$). System III was composed by one copy of the raft-like bilayer surrounded by three copies of the non-raft membrane (*System I*). To build this system we used three replicas of System I and one of the System II (Figure 1(a)). Using the configuration shown in Figure 1(b), the raft-like region remains
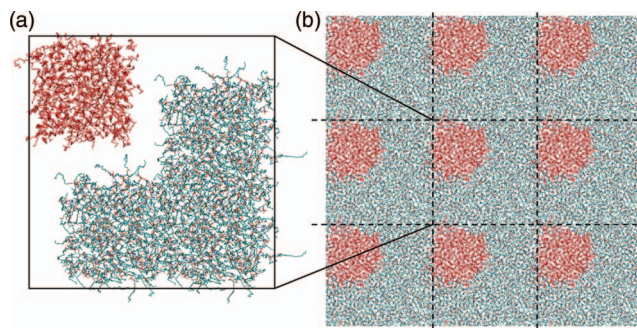

FIG. 1. Building of the raft-like nanodomain. (a) Initial positions of the previously stabilized Systems I and II (blue and red, respectively) prior to the equilibration of the System III. (b) Configuration of the System III after equilibrium under semi-isotropic conditions. The dashed lines indicate the borders of the boundary replicas of the system.

isolated taking profit of the rectangular periodic boundary conditions (PBCs) applied during the simulation. In order to avoid steric clashes, the replica of System II was initially separated by 0.5 nm from any of the three replicas of the System I (Figure 1(a)). The void space between replicas was closed during 10 ns of MD coupling the system to a semi-isotropic barostat (see below). Analogously to Systems I and II, electrolytes were added to simulate physiological conditions (*System III*, Table I). MD simulation of this system was carried out for 400 ns. Notice that the raft-like nanodomain was constructed using the unsaturated DOPC surrounded by lipids with mixed acyl chains (saturated and unsaturated). This was done in order to cover the most relevant lipids found in human erythrocytes[24] and to analyze the properties of a raft domain with unsaturated lipids. After 250 ns of the MD trajectory of *System III*, one parallel simulation was performed in which the DOPC molecules were converted into DSPC (*System III_S*), to analyze the properties of a raft domain with a totally saturated lipid.

Ionic asymmetry.   In all the simulations ions were added to the aqueous compartment in random positions. In the preliminary simulations (symmetric *Systems Ia, Ib, IIb,* and *IIc*) electrolytes were allowed to move freely along the computational box.

To avoid the diffusion of simple electrolytes in *Systems I, II, II_S, III,* and *III_S*, asymmetric concentrations of different ionic species at both sides of the membrane were treated using the BRIM scheme.[28] This method restricts the motion of the ions in the direction perpendicular to the membrane plane. In this way we have the extracellular leaflet highly exposed to Na^+ and Ca^{2+} and the intracellular side highly exposed to K^+. Anions (Cl^-) and a couple of Na^+ and K^+ ions were allowed to freely diffuse in the aqueous solution in those systems. The cutoff used for the restriction of the ionic motion was chosen to be 1.8 nm as it was used and discussed in our previous work.[28] The amount of water molecules in all the cases produced a separation between the average planes of both leaflets (between two consecutive images within the PBC) of nearly 5 nm. This leaves a layer of bulk water with a thickness ≥ 1 nm. Considering that the radial distribution function of any water model relaxes beyond ~0.8 nm, this bulk water layer ensures a reasonable separation between two bilayer replicas. The salt concentrations used for these systems (calculated within the cutoff) roughly represent the extra- and intracellular leaflet, respectively.[25]

Simulation details.   All MD simulations were performed using the Gromacs package version 3.3.3.[37,38] The united atom force field of Berger *et al.*[39] was applied for the phospholipids. All the systems were solvated with SPC water molecules,[40] the ions and the amino acids for the simulation of the protein helix were modeled using the default parameters from the Gromacs force field 53a6.[41] A direct cutoff for non-bonded interactions of 1 nm, and particle mesh Ewald[42,43] for long-range electrostatics were applied. Berendsen baths[44] were used to couple the simulation boxes at a pressure of 1 atm and a temperature of 310 K. The lipid

molecules and water/ions were coupled to separate Berendsen thermostats. Although this thermostat does not reproduce the correct statistical ensemble, this option was chosen since it is commonly used in membrane simulations.[31,34,45,46] Moreover, it was originally used for the parameterization of the Berger force field for the lipids.[39] All bond lengths of the lipid molecules were constrained using the LINCS algorithm[47] whereas the SETTLE algorithm[48] was used for water molecules. The time step was set to 2 fs. Simulations of all the systems were equilibrated during 10 ns of MD. The simulated time for each system is reported in Table I.

The area per lipid was calculated using the Voronoi tessellation technique as it was previously used and described in the literature.[49–52] It must be noticed that the approach used in this work (using only the P atoms) provides only an approximation to the real values since it tends to overestimate the area of smaller molecules and underestimate those of larger ones.[26] Nevertheless, it allows us to obtain a good comparative measure of the area per lipid for each component and their variation upon changes in the conditions and/or composition of the mixture.

The thickness was measured as the average distance between the centers of mass of the phosphorous atoms in each of the two layers. This way to measure the thickness minimizes the errors due to lateral fluctuations as the measure is performed only in the z axis. The obtained errors are quite small in comparison to experimental values since they came from an average value along the trajectory. This gauge was chosen since it is comparable to experimental measurements of the thickness using the Luzzati method[53,54] where the position of the phosphorus group can be interpreted as the location of the Luzzati interface and it is commonly used in membrane simulations.[28,45,55] Contour levels were calculated by mapping the position of the phosphorous atoms onto a 0.5 nm grid (with the positions averaged for all the frames on each monolayer). The order parameters were calculated for the C5 carbons as these positions roughly correspond to the center of the lipid tails and it is in contact with the cholesterol molecules.[32,33] Hence, it is indicative of the cholesterol-induced lipid order. The values obtained were then plotted onto a 2D surface parallel to the membrane (averaged over the last 50 ns of trajectory) as it was done in previous works.[32,33]

The electrostatic potential across the box was computed dividing the system in 100 slices, adding the charges per slice and then integrating twice over this charge distribution. The electrostatic potential was taken to be zero at the walls of the box. Transmembrane potential for Systems I and II was calculated along the direction perpendicular to the membrane.

RESULTS AND DISCUSSIONS

Despite the number of studies performed on membrane systems, very few have been reported in the presence of asymmetric concentration of electrolytes and lipidic mixtures. Aimed to better organize the discussion and get a comparative picture, we describe first the results concerning the non-raft plasma membrane and then those of the raft-like model. Characteristic parameters such as area per lipid, thickness, density profile of the components (along with the ionic

TABLE II. Area per lipid in Å^2 for each of the components of the different systems calculated using the Voronoi tessellation approach.

	DOPC	SGML	CHOL	POPC	POPE	POPS
System Ia	…	…	…	60.3 ± 2.1	…	…
System Ib	…	…	…	…	52.1 ± 1.5	52.7 ± 1.8
System I						
Extra	…	…	…	57.8 ± 0.8	…	…
Intra	…	…	…	…	51.4 ± 1.0	53.7 ± 0.9
System IIa	43.2 ± 1.2	47.5 ± 1.4	36.1 ± 1.2	…	…	…
System IIb	43.1 ± 1.1	47.5 ± 1.6	35.7 ± 1.3	…	…	…
System IIc	43.4 ± 1.0	47.5 ± 1.6	35.7 ± 1.2	…	…	…
System II						
Extra	42.3 ± 1.2	45.1 ± 1.0	37.1 ± 1.1	…	…	…
Intra	42.9 ± 1.3	46.0 ± 1.3	35.7 ± 0.9	…	…	…
System II$_S$						
Extra	41.3 ± 1.3[a]	43.1 ± 1.4	33.8 ± 1.1	…	…	…
Intra	40.4 ± 0.9[a]	44.5 ± 1.3	33.5 ± 1.0	…	…	…
System III						
Extra	43.3 ± 1.3	46.1 ± 1.7	34.4 ± 1.7	57.9 ± 0.5	…	…
Intra	46.7 ± 1.3	45.5 ± 1.4	37.8 ± 1.2	…	50.3 ± 0.8	49.9 ± 1.0
System III$_S$						
Extra	42.5 ± 1.3[a]	47.2 ± 1.3	37.3 ± 1.1	57.3 ± 1.4	…	…
Intra	44.1 ± 1.1[a]	46.8 ± 1.1	37.1 ± 1.1	…	49.5 ± 1.3	51.9 ± 1.6

[a]In these systems DOPC is replaced by DSPC.

distribution) of these two homogeneous mixtures will be taken as reference states. The results obtained from both systems will then be used to construct and analyze the behavior of an inhomogeneous mixture representative of a raft nanodomain inserted in a non-raft context. Finally, we will explore the effects of these three different environments on the orientation of a transmembrane helix of the CD28 receptor.

Homogeneous lipids' mixtures

System I: Non-raft plasma membrane

Area per lipid. The average area per lipid is a typical quantity for membrane systems since it is intimately related to the structure of the bilayer. Owing to the mixture of lipids, the Voronoi tessellation approach[50–52,56] is used to estimate this quantity using the last 50 ns of the simulated trajectory.

The areas per lipid for Systems Ia, Ib, and I are reported in Table II. The values obtained for Systems Ia and Ib (60.3 ± 0.8 Å^2 for POPC and 52.9 ± 1.4 Å^2 for the mixture of POPE and POPS) are coincident with those reported by Gurtovenko and Vattulainen[30] for similar systems (60.4 Å^2 and 51.1 Å^2 for pure POPC in a solution of NaCl and pure POPE in a solution of KCl, respectively).

Owing to the adjustment of the number of phospholipids according to the values obtained from Systems Ia and Ib, the areas per lipid of the components of both leaflets in System I remain practically unchanged (Table II).

Thickness. An important feature in our simulations is the incorporation of ionic asymmetry at both sides of the membrane. As the interaction with cations, especially sodium, introduces an increment of nearly 10% in the thickness,[28,30,57] a realistic representation of the plasma membrane requires

the presence of sodium at the extracellular side and potassium at the intracellular side. This results in the adsorption of sodium ions only on the extracellular leaflet generating a membrane thickness of 4.35 ± 0.04 nm (Table III). The values reported in the literature for the thickness for pure membranes of POPC, POPE, and POPS are 3.7 nm,[58,59] 4.2 nm,[59] and 5.4 nm,[60] respectively. This indicates that the thickness obtained by us for System I is an intermediate of the values of membranes with one single component.

Density profiles. A comprehensive view of the distribution of the different components of the system can be acquired from the number density profile along the z axis calculated for all the systems during the last 50 ns of simulation (Figures 2(a) and 2(b)). Owing to their acidic nature, the POPS molecules are faintly more exposed to the solvent relative to POPE in the intracellular leaflet, as evidenced by a slight right-shift of the density curves. Furthermore, the distribution of the potassium ions shows a peak near (but not adsorbing onto) the intracellular leaflet due to the attraction by acidic head of the POPS molecules, which are exposed to the solvent. On the contrary, the repulsion between the anionic heads

TABLE III. Membrane thickness. Averaged membrane thickness in nm for the different systems and for the different regions of each system.

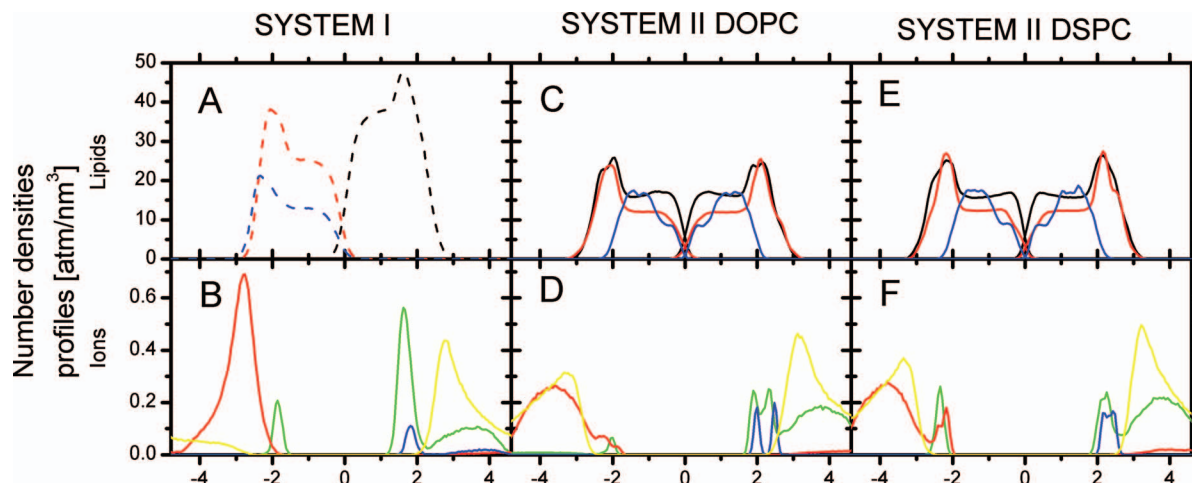|	Plasma membrane region	RAFT region
System I	4.35 ± 0.04	…
System II	…	4.69 ± 0.02
System II$_S$	…	4.93 ± 0.02
System III	4.37 ± 0.03	4.66 ± 0.06
System III$_S$	4.35 ± 0.02	4.78 ± 0.03

FIG. 2. Density profiles. Number density profiles of lipid molecules and electrolytes across the simulation box in the direction perpendicular to the membrane plane. Data are presented for System I (a) and (b), System II (c) and (d), and System II$_S$ (e) and (f), respectively. Lipid molecules are shown in dashed black, red, and blue for POPC, POPE, and POPS, respectively, while the color is straight black, red, and blue for DOPC, SGML, and CHOL, respectively. Density profiles of ions are green, red, blue, and yellow for Na$^+$, K$^+$, Ca^{2+}, and Cl$^-$, respectively. All the atoms for the lipid and the ions were used for the calculation of the density profiles but they were calculated separately for each leaflet.

of POPS and chloride results in a depletion of the latter near the intracellular side of the bilayer (Figure 2(b)). Since chloride ions are not restricted in the space, the electrostatic repulsion with the PS lipids from the intracellular leaflet induces a preferential localization in the neighborhood of the POPC lipids at the extracellular side. A completely different situation is observed for the distribution of sodium. Two sharp peaks are localized at the level of the carbonyl moieties reflecting the adsorption of sodium ions at the border of both leaflets. The difference in the height of the two sharp peaks is a consequence of the asymmetric concentration of sodium at both sides of the membrane (see section Methods). This result in different amounts of ions adsorbed onto each monolayer. A shallower maximum is found at the extracellular space, corresponding to sodium electrolytes, which are free in the solution. Calcium ions, present in a much lower concentration and only near the extracellular side, are adsorbed alike sodium onto the POPC surface. The slight shift to the aqueous region is indicative of a preference to interact with the phosphate moiety rather than with the carbonyl groups.[61] It is worth to notice that due to the relatively small size of the molecular systems, only 2 Ca^{2+} ions are present within the extracellular space. Hence, the statistical significance of the Ca^{2+} binding event is limited.

Systems II and II$_S$: Raft-like plasma membranes

Area per lipid. Simulation of a cholesterol and sphingomielin rich lipid bilayer resulted in considerably different membrane properties respect to those of System I. The area per lipid was measured for each of the components of Systems II and II$_S$ (DOPC or DSPC, SGML, and CHOL) at the extra- and intracellular leaflets (Table II). The values between the simulations with DOPC in the presence and the absence of electrolytes resulted very similar for all the lipids in the intra- and extracellular leaflets, indicating that the electrolyte environment does not significantly influences the structural properties of the raft-like bilayer (see below).

Average areas per lipid of 45.5 Å^2 and 36.0 Å^2 were found in System II for SGML and CHOL molecules, respectively. These values are very close to those reported in the literature for the same molecules in similar systems.[62, 63] However, the area per lipid of DOPC in System II is around 30% smaller than that reported for pure DOPC, probably due to the order induced by SMGL and CHOL resulting in a reduction of the area per lipid. Furthermore, a slight decrease in the area per lipid for all the components is observed when comparing System II with System II$_S$ (Table II), suggesting that the presence of saturated lipids gives place to a more compact (although not fully ordered) membrane configuration.

Thickness. In these systems the membrane structure is rather independent of the presence of free electrolytes in the aqueous solution. This is evident from the negligible differences in the thickness calculated in the presence or absence of ions (Table III). In fact, cations do not interact as strongly with this system as with the non-raft bilayer. It is worth to notice that comparison between these two molecular systems shows that the raft-like patch is nearly half a nanometer thicker than the non-raft model. Since the length of all the lipid tails is identical, this outcome should be ascribed to the ordering effect exerted by cholesterol molecules on the neighboring molecules. This behavior is even more pronounced in the simulation with DSPC (System II$_S$) where the unsaturated tails interacting with the cholesterols and SGML molecules further increase the lipid thickness (Table III).

Density profiles. The density profiles along the axis parallel to the membrane of the raft-like systems reveals a different profile with respect to that of the non-raft bilayer (Figure 2, upper panels). The lack of a zwiterionic moiety in the cholesterol molecules places them deeper in the membrane slab, while SGML and DOPC/DSPC are more exposed to the aqueous solvent as POPC and POPE in System I. Furthermore, the analysis of the membrane structure in terms of

the component's density projected onto a perpendicular axis (Figure 2, upper panels) reveals a slightly higher degree of interdigitation between the lipid tails in the non-raft system. The total number density values measured at z = 0 (the center of the membrane) are 21, 20, and 18 C-atoms/nm^3 for Systems I, II, and II$_S$, respectively. This suggests that the increment in the thickness is not only derived from a more ordered configuration in the saturated versus unsaturated lipid tails, but also from a lower interpenetration of both apposed leaflets.

A comparison of the ionic distribution between the non-raft and raft-like cases (Figures 2(b), 2(d), and 2(f)) shows that potassium is more uniformly distributed within the intracellular space in the raft-like cases versus the non-raft simulation. Since the movement of chloride is not constrained, it is found in roughly the same proportion at both sides of the membrane (Figures 2(d) and 2(f)). This is a clear distinction from the non-raft situation (Figure 2(b)), where the repulsion created by the negative charges of POPS shifts the chloride distribution towards the extracellular leaflet. In contrast, smaller peaks are found when considering the distribution of adsorbing cations (sodium and calcium) in comparison with the non-raft situation. The sharper and smaller peaks observed for Systems II and II$_S$ (with DOPC or DSPC) relative to System I are indicative of a minor number of ions adsorbed. In fact, only 1 calcium and 4 sodium ions are bound to the membrane in each of the two raft-like systems, as compared to the 10 observed for the non-raft bilayer. The molecular level explanation for the less marked ionic interaction with a cholesterol and SGML rich membrane can be easily found. In order to get adsorbed, sodium ions must be simultaneously coordinated by the carbonyl or phosphate moieties of up to four phospholipids. Since the concomitant presence of those functional groups in a cholesterol and SGML rich environment is a rather rare event, the capacity to coordinate ions is expected to be impaired in a raft-like environment.

It has been shown that the transmembrane potential is originated from the accumulation of Na$^+$ ions near the carbonyl moieties of the phosphatidylcholine lipids.[34] In agreement with this, the transmembrane potential in both systems is −70 mV, −10 mV, and −14 mV for Systems I, II, and II$_S$, respectively, pointing to a significantly lower polarization in the raft-like environment. This significant reduction in the transmembrane potential could play a role in the localization of different molecules within rafts. In fact, it has been demonstrated that the membrane potential may modulate the lateral segregation of proteins.[64]

Inhomogeneous lipids' mixture

System III: Raft-like nanodomain

There is clear biochemical evidence for the selective sorting of lipids and self-organization within biomembranes (see for instance van Meer *et al.*[65]). However, the characteristics of the CRDs have been a continuous matter of debate during the last two decades.[6,66] In particular, the size of these segregated domains has not yet been clearly determined. Different experimental techniques, however, have generated continuously decreasing size estimates for stable raft-like domains reaching

the order of a few nanometers.[14] With the aim of investigating the structural and dynamical behavior of such nano-sized CRDs we set up a system containing a 6 nm wide domain embedded in a non-raft environment (Figure 1).

Lipid organization. MD simulation resulted in a plastic but still compact configuration of the raft-like nanodomain. This is evidenced by a comparison of the initial and final configurations of the nanodomain for System III (Figure 3 upper panels) and also for System III$_S$ (Figure 3 lower panels). The raft-like nanodomain showed no tendency to dissociation during any of the simulations. However, the intrinsically slow lateral diffusion of the lipids (in the order of 0.1–0.5 nm^2/μs) makes the sub-microsecond timescale accessible to MD unable to properly assess the stability of the nanodomain. Therefore, we limit our analysis to the differences observed with the reference Systems I and II/II$_S$.

We were not able to pinpoint a clear lipid-order/lipid-disorder interface between the raft-like nanodomain and the non-raft region. However, there is a clear signature of the cholesterol-induced ordering within the CRD. To provide a 3D visualization of this effect, we calculated the order parameters of the carbon atoms at position 5 of the lipid tails. Since these atoms are located roughly in the middle of each monolayer, potentially in contact with cholesterol molecules, their order parameter may be indicative of cholesterol-induced ordering effects. The order parameters were plotted on a contour graph as shown in Figures 4(a)–4(c) for the systems with III and III$_S$. Clearly, the CRD presents a higher ordering than the non-raft region. This effect is more evident at the extracellular leaflet, where there is an obvious signature of the CRD at the central region (Figure 4(a)). This central area shows the higher order parameters (indicative of more structured lipids) while the surrounding regions of the membrane are more disordered. An analogous behavior was found at the intracellular leaflet of System III (Figure 4(b)). However, in this case the differences in the ordering are less marked than in the extracellular monolayer. This is probably due to intermolecular H-bond interactions among the PE lipids that compose this leaflet (see below). Introduction of fully saturated lipid tails in the CRD did not significantly increase the ordering in System III$_S$ (compare Figures 4(b) and 4(c)).

Area per lipid. In line with the relatively small variations in the ordering of the lipids, calculation of the individual areas per lipid showed minor changes in the values obtained for most of the molecular species that compose System III, in comparison with the reference Systems I and II (Table II).

Thickness. The thicknesses obtained for Systems I and II for the non-raft and raft-like regions give essentially the same values, i.e., nearly half a nanometer higher in the raft-like region (Figure 4(d)). This implies that, despite its relatively small size, the nanodomain is able to maintain its elongated structure within a non-raft context. Even though the length of the lipid tails of all the components of the system was chosen to be the same, there are marked differences in
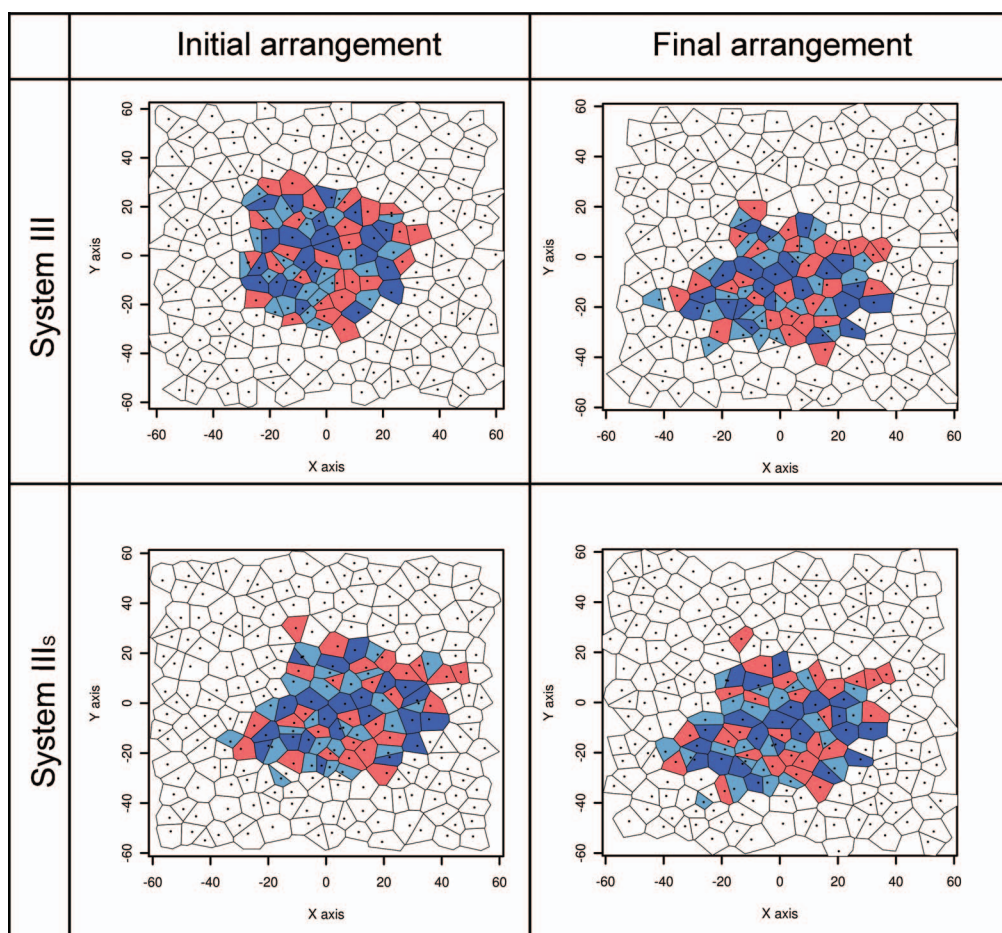
FIG. 3. Voronoi analysis. Voronoi tessellation at the extracellular surface. Initial and final configurations of System III and System III$_S$. The color code is as follow: POPC (white), DOPC or DSPC (red), SGM (blue), and CHOL (light blue).

the intrinsic ordering and thickness between the CRD and the surrounding membrane that arise from the more elongated conformation of the molecules within the nanodomain. It is worth to notice that there is a rough correspondence between the spatial distribution of more ordered lipids and the thickness profile (Figures 4(a) and 4(b)).

An unexpected feature came up when analyzing the contour plot of the thickness calculated for the individual leaflets. While the intracellular leaflet shows a clear elevation of the surface in the CRD patch, this effect is much less evident in the extracellular side (Figures 4(e) and 4(f)). This may originate from the molecular diversity between the phospholipids species at both leaflets. While the bulky choline moiety of POPC is unable to form H-bond interactions, the amine groups of POPE can establish H-bonds with the phosphates and with the COO– of POPS creating a network of electrostatic interactions. This would make the intracellular leaflet more cohesive, helping to reduce the structural distortions introduced by the CRD. In fact, the higher cohesion is reflected by higher order parameters and increased thickness near the center of the intracellular leaflet.

Lateral diffusion. The lateral diffusion coefficients of the different membrane components provide also additional

information that might contribute to the understanding of the behavior of the CRD. Recent evidence from combined atomistic/coarse grained simulations call for caution on the interpretation of the absolute numbers calculated for the diffusion coefficient of phospholipids.[23] We fully agree with these ideas. However, the value of the calculated diffusion coefficients taken in a relative scale within the same set of simulations may furnish a comparative idea of the lateral displacement of different molecular species. Figure 5 shows the values of the diffusion coefficients for all the systems.

Essentially, we found a marked difference in the diffusion coefficients of the non-raft components in both sides of the membrane. As a result of the lack of intermolecular H-bond interactions, the diffusion coefficients of POPCs are clearly more mobile than POPE and POPS in System I (Figure 5(a)). In agreement with this, no relevant differences are observed between the diffusion of molecules at extra- or intracellular side of System II (Figure 5(b)), where the intermolecular electrostatic interactions are expected to be less relevant. The diffusion coefficients for the components of System III (Figure 5(c)) show intermediate values between Systems I and II. This probably suggests a connection between the CDR and its lipidic environment, which tends to reduce the diffusion on the non-raft regions and increase that of the CRD components (in comparison with the reference systems).
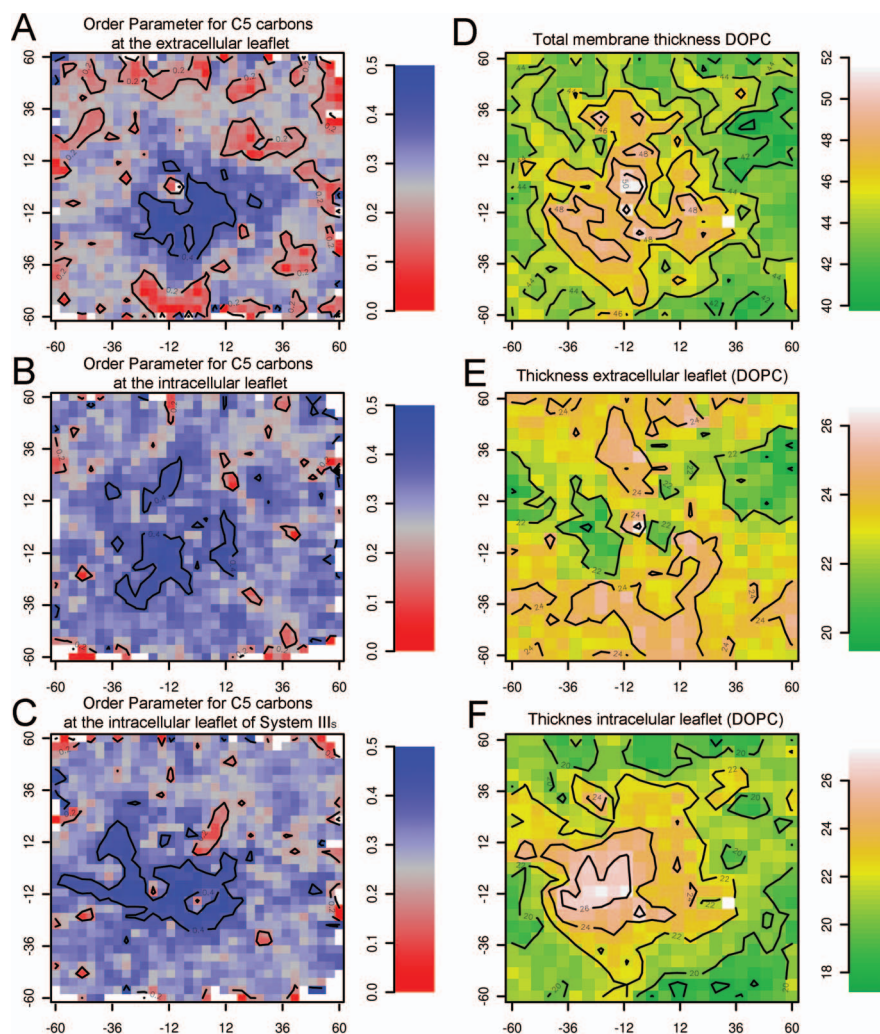
FIG. 4. Order parameter and thickness of the raft-like nanodomain. Order parameters for the carbon atoms at position 5 in the lipid tails of System III: (a) extracellular leaflet of System III. (b) Intracellular leaflet if System III. (c) Intracellular leaflet of System III$_S$. Membrane thickness: (d) total thickness calculated on both layers of System III. (e) and (f) thickness calculated on the extra- and intracellular monolayers of System III, respectively. Notice that the scale in (e) and (f) is different from that used in (d). All the maps were calculated using the last 50 ns of each trajectory.

Long range effects. The planar representation of the order parameter and thickness presented in Figure 4 allows for visual assessment of the perturbation introduced by the raft-like nanodomain in its neighboring regions. To acquire a perspective on how or if the presence of the CRD modifies its neighboring regions it may be useful to compare the order parameters in the different systems studied. The order parameter at the C5 carbons of POPC (at the extracellular leaflet) is 0.23, while 0.29 was measured for both POPE and POPS (at the intracellular leaflet). For System II instead, 0.35 and 0.42 were found for DOPC and SGML, respectively, at both leaflets. The order parameters at the C5 atoms in the non-raft and raft regions (Figures 4(a)–4(c)) are similar to those System I and II, respectively. Similarly, if we analyze the changes in the thickness introduced by the raft-like nanodomain, it results that the perturbations in this quantity do not propagate outside the raft-like patch. In fact, comparison of the thickness calculated, taking non-raft and raft-like components separately into account, reveals nearly the same values for both cases (Table III).

The situation is different if we consider the diffusion coefficients (Figure 5). In this case the values change among the different systems, being those of System III intermediate between System I and System II.
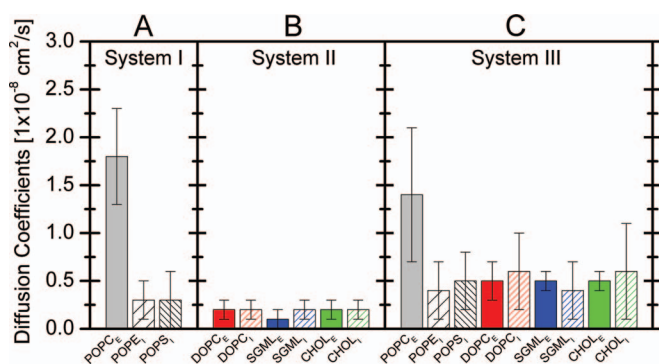

FIG. 5. Diffusion coefficients: bar graph showing the diffusion coefficients for the Systems I (a), II (b), and III (c). The extra- and intracellular components are identified with solid and hollow bars, respectively.

Taking all together, we observe that the lipids can rapidly adapt to the very near environment, converging to unperturbed values within the relatively small dimensions of the simulation box. However, the slower dynamics associated with the lateral diffusion is dumped by the presence of the CRD that reduces the diffusion of the non-raft lipids. Hence, only the slower dynamics associated with the lateral movements is modified. The perturbations on the fast dynamics associated with the order parameters and the increment in thickness exerted by the CRD do not propagate far away from it.

Protein-lipid interactions

Raft domains act as platforms to recruit specific proteins. Owing to the differences in thickness between the non-raft and raft lipids, the hydrophobic mismatch (i.e., the difference between the thickness of the membrane and the length of the hydrophobic helix)[27,67,68] could play a role in mediating lipid-protein interactions. It is, therefore, important to determine if these interactions may be relevant to modulate protein conformations. Moreover, it would also be interesting to know if small raft-like patches, as that studied here, may exert the same effect than an extended raft domain.

It has been shown that the transmembrane domain of the CD28 receptor cooperates in the recruitment and organization of relatively reduced raft patches to create extensive raft platforms for protein-protein interactions at the immunological synapses.[20,69,70] It is therefore conceivable that reciprocal lipid-protein interactions may help to create optimal conditions for protein-protein contacts. In order to address this hypothesis, the transmembrane segment of the CD28 (only one helix) was modeled as a canonical α-helix and inserted into Systems I, II_S, and III_S. Already after only 10 ns of simulation the helical segment reached an orientation of the main axis with respect to the membrane plane, which resulted characteristic for each system (Figure 6). Owing to hydrophobic mismatch, CD28 remained near perpendicular to the bilayer in the case of an extended raft-like membrane (System II_S). It presented a small tilt when inserted in the raft-like nan-

odomain (around 25°) and adopted a more marked inclination (around 50°) in the non-raft environment. It has recently been shown that protein sorting in different subcellular membranes, is intimately related to the length of transmembrane segments.[71] In line with these findings, our results indicate that proteins are able to sense the membrane environment and that despite the reduced dimensions of raft-like nanodomain it may still be capable to modify the orientation of hosted proteins.

Finally, we notice that although hydrophobic mismatch can contribute to the sorting mechanism, electrostatic interactions may also play a role in the localization of proteins. Indeed, the absence of negatively charged species within the raft-like nanodomain and the depletion of ions adsorbed onto this region may generate a signature in the electrostatic profile in the CRD neighborhood.

CONCLUSIONS

Cell membranes exhibit an amazing variety of components that can spontaneously associate giving rise to a multiplicity of phases with different structural and dynamical characteristics. Domains rich in cholesterol and sphingomielin have been the target of a vast amount of research as they create "functional heterogeneities in cell membranes,"[72] which are of outmost relevance in biological processes.[73] However, this kind of systems poses a number of problems to experimental determination.[15,74]

In an effort to contribute to fill this gap, we have presented in this work a series of molecular simulations addressing the molecular nature of a nano-sized CRD, its interactions with surrounding lipids in the environment and with a transmembrane protein helix.

As a first conclusion, we observe that explicit consideration of lipidic and electrolytic asymmetry at both sides of the membrane result in different structural and dynamic behaviors for both leaflets, independently of the presence/absence of a CRD. Our results support the idea that even at the smallest estimated dimensions, nano-sized raft-like domains can still keep the distinctive features of extended rafts. Additionally, they suggest that the ionic distribution at the membrane rim changes in the neighborhood of a CRD.

These results provide some insights on how proteins might sense the presence of these domains. Not surprisingly, CRDs can be easily recognized by their sensibly higher thickness and ordering properties.

Despite the limitations of theoretical techniques in terms of limited spatiotemporal sampling, the results presented provide molecular level insights and further support the idea that nano-sized raft domains have the capacity to host membrane proteins in a (slightly) suboptimal environment. Upon activation, these proteins can be recruited by connections triggered by the cytoskeleton to hot spots, therefore creating an extended, functional platform for protein-protein interactions.[75]
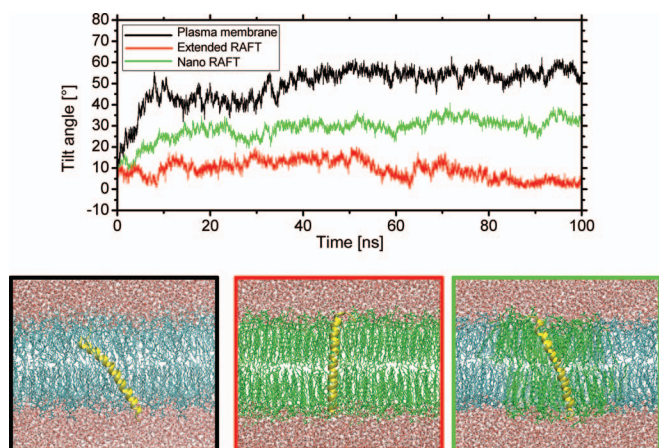

FIG. 6. Protein-membrane interactions: (a) time evolution of the tilt angle of the CD28 transmembrane helix with respect to the membrane plane for the protein inserted in System I (black, top), II (red, bottom), and III (green, middle). Bottom panels show the final snapshots of each system after 100 ns.

[1] S. J. Singer and G. L. Nicolson, Science **175**, 720 (1972).
[2] C. S. Ejsing, J. L. Sampaio, V. Surendranath, E. Duchoslav, K. Ekroos, R. W. Klemm, K. Simons, and A. Shevchenko, Proc. Natl. Acad. Sci. U. S. A. **106**, 2136 (2009).
[3] K. Simons and E. Ikonen, Nature (London) **387**, 569 (1997).
[4] L. J. Pike, Biochem. J. **378**, 281 (2004).
[5] M. Edidin, Annu. Rev. Biophys. Biomol. Struct. **32**, 257 (2003).
[6] S. Munro, Cell **115**, 377 (2003).
[7] K. Jacobson, O. G. Mouritsen, and R. G. Anderson, Nat. Cell Biol. **9**, 7 (2007).
[8] A. S. Shaw, Nature Immunol. **7**, 1139 (2006).
[9] L. Opilik, T. Bauer, T. Schmid, J. Stadler, and R. Zenobi, Phys. Chem. Chem. Phys. **13**, 9978 (2011).
[10] A. Vidal and T. J. McIntosh, Biophys. J. **89**, 1102 (2005).
[11] C. Eggeling, C. Ringemann, R. Medda, G. Schwarzmann, K. Sandhoff, S. Polyakova, V. N. Belov, B. Hein, M. C. von, A. Schonle, and S. W. Hell, Nature (London) **457**, 1159 (2009).
[12] I. A. Prior, C. Muncke, R. G. Parton, and J. F. Hancock, J. Cell Biol. **160**, 165 (2003).
[13] R. G. Parton and J. F. Hancock, Trends Cell Biol. **14**, 141 (2004).
[14] D. Goswami, K. Gowrishankar, S. Bilgrami, S. Ghosh, R. Raghupathy, R. Chadda, R. Vishwakarma, M. Rao, and S. Mayor, Cell **135**, 1085 (2008).
[15] A. Kusumi, Y. M. Shirai, I. Koyama-Honda, K. G. Suzuki, and T. K. Fujiwara, FEBS Lett. **584**, 1814 (2010).
[16] M. Cebecauer, D. M. Owen, A. Markiewicz, and A. I. Magee, Biochem. Soc. Trans. **37**, 1056 (2009).
[17] C. A. Day and A. K. Kenworthy, Biochim. Biophys. Acta **1788**, 245 (2009).
[18] A. Kusumi, C. Nakada, K. Ritchie, K. Murase, K. Suzuki, H. Murakoshi, R. S. Kasai, J. Kondo, and T. Fujiwara, Annu. Rev. Biophys. Biomol. Struct. **34**, 351 (2005).
[19] K. Murase, T. Fujiwara, Y. Umemura, K. Suzuki, R. Iino, H. Yamashita, M. Saito, H. Murakoshi, K. Ritchie, and A. Kusumi, Biophys. J. **86**, 4075 (2004).
[20] R. Tavano, R. L. Contento, S. J. Baranda, M. Soligo, L. Tuosto, S. Manes, and A. Viola, Nat. Cell Biol. **8**, 1270 (2006).
[21] S. Wieser, M. Axmann, and G. J. Schutz, Biophys. J. **95**, 5988 (2008).
[22] D. V. Nicolau, Jr., K. Burrage, R. G. Parton, and J. F. Hancock, Mol. Cell Biol. **26**, 313 (2006).
[23] T. Apajalahti, P. Niemela, P. N. Govindan, M. S. Miettinen, E. Salonen, S. J. Marrink, and I. Vattulainen, Faraday Discuss. **144**, 411 (2010).
[24] D. E. Vance and J. E. Vance, *Biochemistry of Lipids, Lipoproteins and Membranes*, 4th ed. (Elsevier Science, Amsterdan, 2002), Chap. 1.
[25] B. Alberts, A. Johnson, J. Lewis, M. Raff, K. Roberts, and P. Walter, *The Molecular Biology of the Cell*, 4th ed. (Garland Science, New York, 2002).
[26] S. A. Pandit, E. Jakobsson, and H. L. Scott, Biophys. J. **87**, 3312 (2004).
[27] S. Ramadurai, A. Holt, L. V. Schafer, V. V. Krasnikov, D. T. Rijkers, S. J. Marrink, J. A. Killian, and B. Poolman, Biophys. J. **99**, 1447 (2010).
[28] F. E. Herrera and S. Pantano, J. Chem. Phys. **130**, 195105 (2009).
[29] W. Zhao, T. Rog, A. A. Gurtovenko, I. Vattulainen, and M. Karttunen, Biophys. J. **92**, 1114 (2007).
[30] A. A. Gurtovenko and I. Vattulainen, J. Phys. Chem. B **112**, 1953 (2008).
[31] A. A. Gurtovenko, M. Miettinen, M. Karttunen, and I. Vattulainen, J. Phys. Chem. B **109**, 21126 (2005).
[32] P. S. Niemela, S. Ollila, M. T. Hyvonen, M. Karttunen, and I. Vattulainen, PLoS Comput. Biol. **3**, e34 (2007).
[33] P. S. Niemela, M. T. Hyvonen, and I. Vattulainen, Biochim. Biophys. Acta **1788**, 122 (2009).
[34] S. J. Lee, Y. Song, and N. A. Baker, Biophys. J. **94**, 3565 (2008).
[35] A. A. Gurtovenko and I. Vattulainen, J. Phys. Chem. B **112**, 4629 (2008).
[36] D. P. Tieleman and H. J. Berendsen, Biophys. J. **74**, 2786 (1998).
[37] H. J. C. Berendsen, D. van der Spoel, and R. van Drunen, Comput. Phys. Commun. **91**, 43 (1995).
[38] E. Lindahl, B. Hess, and D. van der Spoel, J. Mol. Model. **7**, 306 (2001).
[39] O. Berger, O. Edholm, and F. Jahnig, Biophys. J. **72**, 2002 (1997).
[40] H. J. C. Berendsen, J. P. M. Postma, W. F. van Gunsteren, and J. Hermans, in *Intermolecular Forces*, edited by B. Pullman (D. Reidel Publishing Company, Dordrecht, 1981), pp. 331–342.
[41] C. Oostenbrink, T. A. Soares, N. F. van der Vegt, and W. F. van Gunsteren, Eur. Biophys. J. **34**, 273 (2005).
[42] T. Darden, D. York, and L. G. Pedersen, J. Chem. Phys. **98**, 10089 (1993).
[43] U. Essman, L. Perela, M. L. Berkowitz, T. Darden, H. Lee, and L. G. Pedersen, J. Chem. Phys. **103**, 8577 (1995).
[44] H. J. C. Berendsen, J. P. M. Postma, W. F. van Gunsterren, A. DiNola, and J. R. Haak, J. Chem. Phys. **81**, 3684 (1984).
[45] D. Poger, W. F. van Gunsteren, and A. E. Mark, J. Comput. Chem. **31**, 1117 (2010).
[46] M. S. Miettinen, A. A. Gurtovenko, I. Vattulainen, and M. Karttunen, J. Phys. Chem. B **113**, 9226 (2009).
[47] B. Hess, H. Bekker, H. J. Berendsen, and J. Fraaije, J. Comput. Chem. **18**, 1463 (1998).
[48] S. Miyamoto and P. A. Kollman, J. Comput. Chem. **13**, 952 (1992).
[49] S. A. Pandit, S. Vasudevan, S. W. Chiu, R. J. Mashl, E. Jakobsson, and H. L. Scott, Biophys. J. **87**, 1092 (2004).
[50] P. Jedlovszky, J. Phys. Chem. B **108**, 465 (2004).
[51] E. Falck, M. Patra, M. Karttunen, M. T. Hyvonen, and I. Vattulainen, Biophys. J. **87**, 1076 (2004).
[52] W. Shinoda and S. Okazaki, J. Chem. Phys. **109**, 1517 (1998).
[53] V. Luzzati, in *Biological Membranes*, edited by D. Chapman (Academic, London, 1968), pp. 71–123.
[54] J. F. Nagle and S. Tristram-Nagle, Biochim. Biophys. Acta **1469**, 159 (2000).
[55] M. Rappolt, A. Hickel, F. Bringezu, and K. Lohner, Biophys. J. **84**, 3111 (2003).
[56] M. Patra, M. Karttunen, M. T. Hyvonen, E. Falck, P. Lindqvist, and I. Vattulainen, Biophys. J. **84**, 3636 (2003).
[57] R. A. Bockmann, A. Hac, T. Heimburg, and H. Grubmuller, Biophys. J. **85**, 1647 (2003).
[58] J. F. Nagle, R. Zhang, S. Tristram-Nagle, W. Sun, H. I. Petrache, and R. M. Suter, Biophys. J. **70**, 1419 (1996).
[59] S. Leekumjorn and A. K. Sum, J. Phys. Chem. B **111**, 6026 (2007).
[60] P. Mukhopadhyay, L. Monticelli, and D. P. Tieleman, Biophys. J. **86**, 1601 (2004).
[61] X. L. Iraolagoitia and M. F. Martini, Colloids Surf., B **76**, 215 (2010).
[62] P. R. Maulik and G. G. Shipley, Biochemistry **35**, 8025 (1996).
[63] P. R. Maulik, D. Atkinson, and G. G. Shipley, Biophys. J. **50**, 1071 (1986).
[64] G. Grossmann, M. Opekarova, J. Malinsky, I. Weig-Meckl, and W. Tanner, EMBO J. **26**, 1 (2007).
[65] G. van Meer, D. R. Voelker, and G. W. Feigenson, Nat. Rev. Mol. Cell Biol. **9**, 112 (2008).
[66] D. Lingwood and K. Simons, Science **327**, 46 (2010).
[67] J. A. Killian, Biochim. Biophys. Acta **1376**, 401 (1998).
[68] T. M. Weiss, P. C. van der Wel, J. A. Killian, R. E. Koeppe, and H. W. Huang, Biophys. J. **84**, 379 (2003).
[69] R. Tavano, G. Gri, B. Molon, B. Marinari, C. E. Rudd, L. Tuosto, and A. Viola, J. Immunol. **173**, 5392 (2004).
[70] C. Wulfing and M. M. Davis, Science **282**, 2266 (1998).
[71] H. J. Sharpe, T. J. Stevens, and S. Munro, Cell **142**, 158 (2010).
[72] D. Lingwood, H. J. Kaiser, I. Levental, and K. Simons, Biochem. Soc. Trans. **37**, 955 (2009).
[73] K. Simons and M. J. Gerl, Nat. Rev. Mol. Cell Biol. **11**, 688 (2010).
[74] R. Lindner and H. Y. Naim, Exp. Cell Res. **315**, 2871 (2009).
[75] S. Mayor, A. Viola, R. V. Stan, and M. A. del Pozo, EMBO Rep. **7**, 1089 (2006).